IOPscience

HOME | SEARCH | PACS & MSC | JOURNALS | ABOUT | CONTACT US

Evidence of thermal and non-thermal mechanisms coexisting in dense plasma focus D-D nuclear reactions

This article has been downloaded from IOPscience. Please scroll down to see the full text article.

2000 J. Phys. D: Appl. Phys. 33 141

(http://iopscience.iop.org/0022-3727/33/2/308)

The Table of Contents and more related content is available

Download details:
IP Address: 200.5.106.13
The article was downloaded on 01/07/2009 at 20:04

Please note that terms and conditions apply.

J. Phys. D: Appl. Phys. **33** (2000) 141–147. Printed in the UK PII: S0022-3727(00)06103-9

Evidence of thermal and non-thermal mechanisms coexisting in dense plasma focus D–D nuclear reactions

F Castillo†, M Milanese‡, R Moroso and J Pouzo‡

Instituto de Física Arroyo Seco, Universidad Nacional del Centro, (7000) Tandil, Argentina

Received 19 July 1999, in final form 8 October 1999

Abstract. Dense plasma foci are the most efficient devices in the production of fast neutrons proceeding from deuterium nuclear fusion reactions. This work deals with experiments in a small plasma focus machine and attempts to distinguish neutrons of thermal origin from non-thermal neutrons, and the search for possible sources of both.

Soft x-rays emitted by bremsstrahlung in a plasma focus were experimentally studied, using a multiple pin-hole camera with different aluminium absorbers in each hole. This method allows one to obtain the time-integrated soft x-ray image, as well as an estimation of the mean electronic temperature. The time-resolved soft x-ray intensity is registered with a filtered p-intrinsic-n (PIN) diode detector, shielded with a beryllium sheet. The time-resolved hard x-ray intensity (associated with particle acceleration) was registered using a plastic scintillator coupled to a fast photomultiplier tube. With a similar system, the time-resolved neutron emission is also registered. From the soft x-ray photographic studies, bright points with temperatures two or three times higher than the bulk plasma temperature are observed. These bright points (one or two per focus) can reach temperatures of over 7 keV, and their formation seems to correlate with successive necking produced by $m = 0$ instabilities in the pinch column. Time-integrated and time-resolved measurements of neutron yield, performed in comparison with time-resolved measurements of soft and hard x-ray radiation, show the different influence of thermal and non-thermal mechanisms in the nuclear fusion reactions.

1. Introduction

In a dense plasma focus device [1] a high-voltage discharge of a capacitor bank is produced (through a spark-gap switch) in a coaxial electrode gun surrounded by a filling gas at a pressure of some millibar (see figure 1). A plasma sheath is generated on the insulator which separates both electrodes (normally Pyrex glass or alumina ceramic) and travels along the coaxial cavity. At the end of the gun, a radial implosion begins, moves towards the gun axis and forms a cylinder-shaped of plasma (focus), which is a few centimetres long and several millimetres in diameter. The focus has a duration of about 100 ns, in which the plasma reaches a temperature of several kilo electronvolts and a density n of about 10^{19} cm^{-3}. From the Spitzer expression [2] at $n \sim 10^{19}$ cm^{-3} and the electron temperature $T_e \cong 1$ keV, the equipartition time is around 10^{-8} s. Under such conditions, the deuteron temperature is close to the electron temperature, and then the hypothesis of $T_e \sim T_i$ can be accepted.

If the filling gas in the discharge chamber is deuterium at an appropriate density, fusion neutrons (n in the following equation) from the nuclear reaction D + D $\rightarrow$ ^{3}He + n are emitted in the focus. The plasma sheath, or current sheath (CS), dynamics depends on: the electrical parameters of the discharge circuit, on the electrode geometry and, essentially, on the neutral gas density.

There are two main mechanisms for fusion reactions in plasma focus devices. The first is a thermal mechanism for which the D–D reactions are produced by the thermal collisions between deuterons in the bulk of the plasma focus. The second is the reaction produced by accelerated (suprathermal) deuterons colliding with the thermal deuterons in the plasma bulk and/or the neutral gas atoms outside the plasma (beam-target effect). A large number of measurements show that the neutron and electromagnetic radiation (x-rays, microwaves) emission spectra from plasma focus devices are characterized by a marked anisotropy [1, 3–5]. This fact suggests that non-thermal processes, such as the beam-target effect, may play an important role in the fusion mechanism. A detailed calculation of the anisotropy of the neutron flux and the spectra for plasmas with anisotropy was made in classic works of Lehner and Pohl [6] and Cipolla [7]. There are essentially two causes of the neutron anisotropy. The first is the velocity of mass-centre of colliding deuterons is preferentially in the electrodes' axial direction and causes the anisotropy in the laboratory system. The other reason

† Fellow of CONICET-Argentina. Permanent address: Instituto de Ciencias Nucleares UNAM, A. P. 70543, Mexico D. F. Mexico.
‡ Member of the Research Career of CONICET-Argentina.

 © 2000 IOP Publishing Ltd

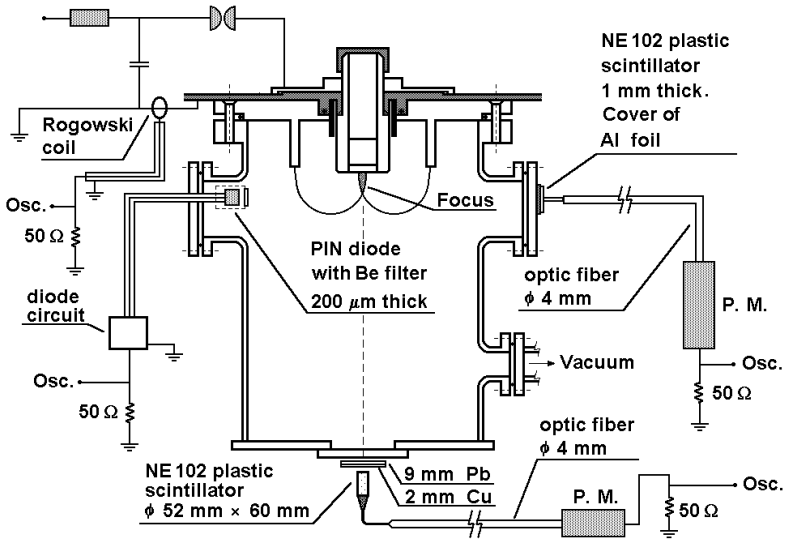

Figure 1. Schematic diagram of the plasma focus device and experimental set-up showing two of the four lateral windows for side-on diagnostics and the frontal window for end-on diagnostics. Side-on diagnostics uses time-resolved soft x-ray (PIN diode detector) and time-resolved hard x-ray (scintillator–photomultiplier system) and end-on diagnostic uses time-resolved neutron signal. The photomultiplier is labelled P.M.

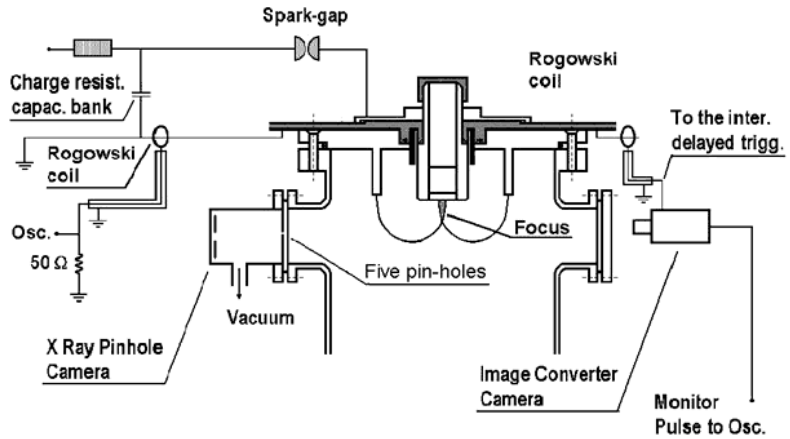

Figure 2. Schematic diagram showing the other two lateral windows (the discharge chamber is here rotated 90° respect to figure 1) for side-on diagnostics; the image converter camera and time-integrated soft x-ray five-pinhole camera are shown.

for anisotropy occurs because the differential cross section in the mass centre system for the nuclear fusion reaction: D + D $\rightarrow$ ^{3}He + n can be described by [8]

$$\frac{\mathrm{d}\sigma}{\mathrm{d}\omega^*} = \left(\frac{\mathrm{d}\sigma}{\mathrm{d}\omega^*}\right)_{\theta^*=\pi/2} (1 + A(E_R)\cos^2\theta^*)$$

where $\mathrm{d}\omega^*$ is the solid angle in the mass centre system, θ^* is the angle between the relative velocity of colliding deuterons and the neutron velocity in the mass centre system; $A(E_R)$ is a coefficient dependent on the relative deuteron energy. Thus, if the relative velocity does not have a random component, there is a stronger activity in a particular direction. Moreover, if the relative velocity is randomly oriented (such as in the 'moving boiler' model [9]) the anisotropic differential cross section has no effect.

The x-ray emission characteristics depend strongly on the electrode configuration, power supply systems and the gaseous pressure conditions. These characteristics are relevant, not only for basic plasma studies, but also for different technological applications such as radiography, x-ray microscopy and lithography.

Two different sources of x-ray emission are present during focus evolution [10, 11]. The first is a soft x-ray source in the focused plasma column which emits by electron bremsstrahlung in the thermal energy range. Generally, this source is characterized by a low-energy spectrum (a few keV) and it is normally associated with the thermal fusion mechanism. The second, a hard x-ray source, results from the electron collisions of the centre electrode by electron beams axially emitted from the focus. The energy spectrum of these electrons covers a wide range (several hundred keV) [12] and, due to such high energies, this emission is considered to originate from non-thermal processes.

The existence of very small regions of intense soft x-ray emission within the hot dense plasma in a plasma focus, has been detected and reported [13, 14, 15]. It was observed that these plasma spots are positioned roughly along the

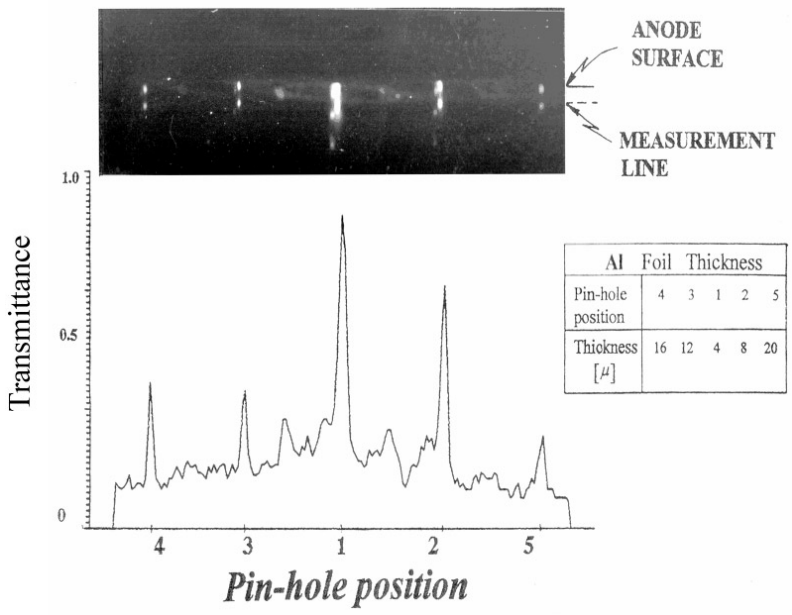

Figure 3. A five-pinhole camera photograph and the corresponding transmittance curve.

focus current channel. It was mentioned that they resembled the $m = 0$ instability in a pinched discharge. Several studies show that these localized emission regions (hot-spots) could be observed as bright spots or elongated micropinches [13].

In the present work we study, through soft x-ray detectors, the presence of small regions of intense x-ray radiation, of low energy, in the plasma column. We also study the possible existence of both mechanisms (thermal and non-thermal) through measurement of the neutron yield (average value) Y, in comparison with time-resolved intensity measurements of soft and hard x-ray radiation. The experimental results give confirmation of the coexistence of both mechanisms, and show the possible competition between them for the plasma focus neutron yield.

2. Experimental systems and methods

The dense plasma focus machine used is a device named PACO [16], with 2 kJ of energy in the capacitor bank when it is operated at a voltage of 31 kV. At this voltage the maximum discharge current I (in the focus) reaches 250 kA and, using D_2 at 1.5 mb as the filling gas, the fusion neutron yield results in average $\sim 4 \times 10^8$ per shot. Time integrated measurement of neutrons is performed with two silver activation counters located in directions perpendicular to the gun axis. The average of Y emitted in 4π sr was calculated by averaging the counts of both detectors, which present the same solid angle of detection. The duration of the neutron pulse, measured with a scintillator–photomultiplier detector, is about 50 ns in this device. A Rogowski coil registers the derivative of the discharge current ($\mathrm{d}I/\mathrm{d}t$). The typical dip in the signal due to the focalization of the discharge indicates that the CS time from run-down up to the focus is of about 1.2 μs. The time-integrated soft x-ray images of the plasma column were obtained using a pinhole camera. Simultaneously, time-resolved measurements of this x-ray emission were performed with a fast p-intrinsic-n (PIN) diode detector. In addition, the hard x-ray signal from the NE-102 A scintillator detector placed side-on or in front of the gun's z-axis was registered. A schematic diagram of the device and experimental set-up for the different diagnostics are shown in figures 1 and 2.

The five-pinhole x-ray camera (its location in the vacuum chamber can be seen in figure 2) consists of a compartment for housing two soft x-ray sensitive films (Kodak direct exposure film (DEF)), which is connected to the pinhole holder through a brass tube. In this camera, a vacuum of around 10^{-3} Torr is produced in order to reduce the absorption of x-rays by air. The five pinholes, each of 200 μm diameter, are made on a 0.2 mm thick silver sheet. The pinholes are arranged in a straight line, perpendicular to the gun axis, with a separation of 4.5 mm between each pinhole. Al foil filters are attached over each hole. The thickness of the foils are 4, 8, 12, 16 and 20 μm. The x-ray flux collected by this pinhole camera was enough to produce images on the DEF in a single discharge; at least through the three holes with thinnest filters. X-ray photographs can be taken in two successive discharges, with the camera remaining under vacuum, by rotating its back side, where the two corresponding DEF plates are attached, one half-turn. The Kodak DEF has been studied extensively [17] and presents an almost linear response with the intensity of x-rays in the energy range of 1–10 keV. This allows one to obtain (as described in the next section) an estimation of the plasma electron temperature T_e from measurements of the total x-ray intensity by densitometry of the light intensity on the photographic film. The densitometry of the exposed film was performed taking the images with a charge-coupled device (CCD) camera and processing them with a special computer program, which gives the relative transmittance of the negative plate with a spatial resolution, on the plate, of 0.13 mm. This represents a resolution

of 0.32 mm at the plasma. The intensity of each point corresponds to spatially-integrated light, in the direction of observation, over a distance of, at most, about 1 mm (the diameter of the plasma column) and to time-integrated light of a duration of 20 ns (duration of each soft x-ray burst, taken from the PIN diode oscillograms). In figure 3, a typical photograph with the five x-ray images of the plasma emitting zones, and the corresponding curve of transmittance obtained in a line perpendicular to the gun axis, can be observed.

The experimental set-up for the time-resolved x-ray and neutron pulse registrations is shown in figure 1. The temporal evolution of the soft x-ray emission (spatially integrated) was registered using a fast PIN diode (response time of 0.5 ns). The diode was shielded with a 200 μm thick beryllium window, in order to stop the visible light of the plasma. It was located in a side-on position (perpendicular to the gun axis).

The time-resolved measurements of the hard x-ray emission was registered using a NE-102 plastic scintillator, coupled to a photomultiplier, Phillips 150 AVP tube, via a 4 mm diameter optical fibre. The use of this optical fibre connection allows us to place the photomultiplier in a Faraday cage and, in this way, minimize the electromagnetic noise in the signal. The scintillator used in these measurements was 0.5 mm thick in order to minimize the effect of the D–D fusion neutrons (at this thickness the scintillator efficiency for neutrons of 2.45 MeV is practically zero). The scintillator was covered with Al foil to shield it from visible light and was located outside the discharge chamber in front of a 4 mm thick glass window (see figure 1). This window represents a filter for x-rays with energies below 30 keV; therefore, this is the lower energy threshold in our hard x-ray measurements.

The time-resolved measurements of neutrons were performed with the same detector system (scintillator–optical fibre–photomultiplier), but the dimension of the scintillator was 52 mm in diameter and 60 mm long and it was coupled to the optic fibre through a conical light guide. The scintillator was located 1 m in front of the anode end (outside the chamber) and hard x-rays were stopped with a Pb–Cu combined filter: using a thickness of 9 mm Pb and 2 mm Cu there were no transmission of x-ray pulses. This combined filter has its threshold at 500 keV; therefore, it gives an estimation of the upper energy limit of the hard x-ray emission in our device.

All of the signal delays produced by the transmission lines (including the optic fibre's delay) are measured and compensated for in order to register the events simultaneously in a multichannel oscilloscope, resulting in a timing that is better than 3 ns.

As a reference time for time measurements of all signals, the $\mathrm{d}I/\mathrm{d}t$ dip (negative peak) Rogowski coil method was used. This procedure is justified because this time corresponds to the minimum pinch diameter, as was studied in a previous work reported in [18] (see figure 10 of [18]).

In figure 4, two typical oscilloscope registers of the signals (from Tektronix TDS 540 A) are shown, displaying from top to bottom, figure 4(a) soft x-rays, hard x-rays and in the Rogowski $\mathrm{d}I/\mathrm{d}t$ and figure 4(b) soft x-rays, neutrons and $\mathrm{d}I/\mathrm{d}t$. In the group of traces in figure 4(b) it can be observed that the maximum of the neutron pulse $Y(t)$ appears 50 ns after the $\mathrm{d}I/\mathrm{d}t$ dip, the time corresponding to the time-of-flight of 2.45 MeV neutrons from the focus to the scintillator (50 ns m^{-1}). This fact represents an extra confirmation that we are registering the neutron pulse without superposition of hard x-ray emission (which is stopped completely by the Pb–Cu filter).

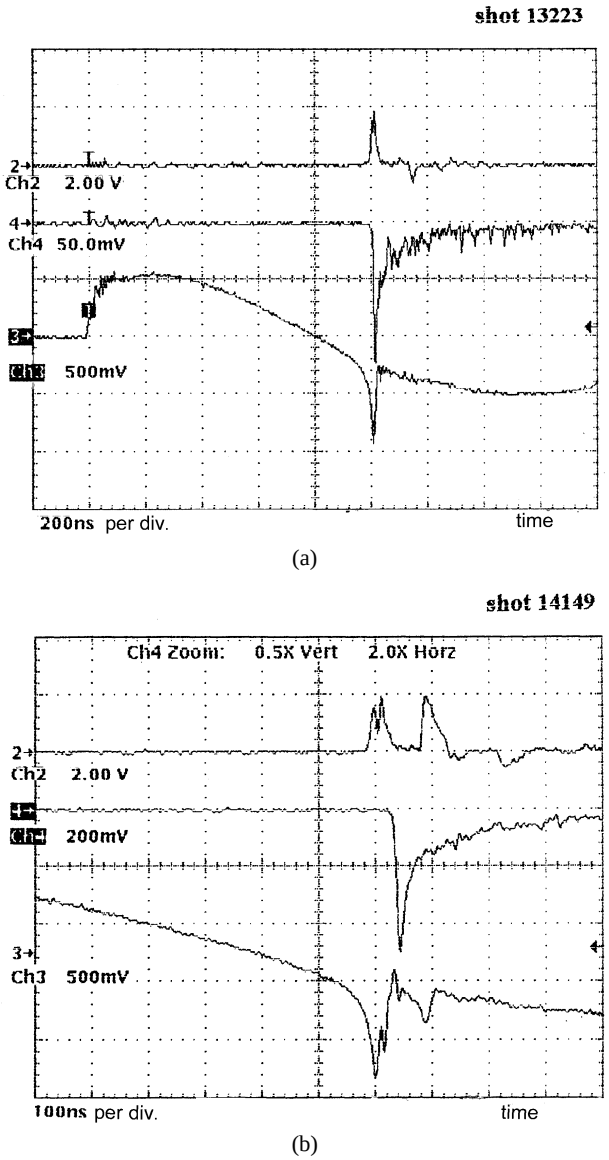

Figure 4. Oscillograms of typical shots showing three simultaneous diagnostics: (a) shot 13223: upper trace (channel 2) corresponds to the PIN diode signal (soft x-ray pulse); middle trace (channel 4) corresponds to the thin scintillator–photomultiplier signal (hard x-ray pulse); and the lower trace (channel 3) corresponds to the Rogowski coil signal (total current derivative). (b) shot 14149: Upper trace (channel 2) corresponds to the PIN diode signal (soft x-ray); middle trace (channel 4) corresponds to the thick scintillator signal with an Al–Cu filter (neutron pulse detector) and the lower trace (channel 3) corresponds to the Rogowski coil signal (total current derivative).

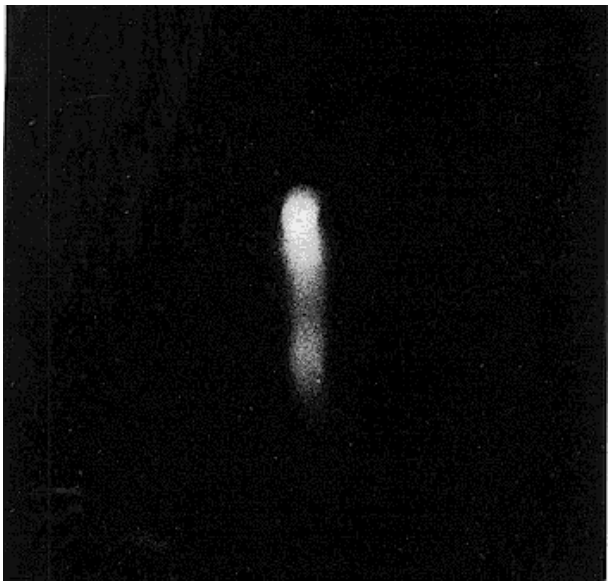

Figure 5. An x-ray emission picture amplified (×6).

3. Results and comments

3.1. The soft x-ray photographs

In figure 5 we show an amplified photograph of a pinch x-ray image, in which a bright point can be observed. We assume here quasi-thermal equilibrium in the focus in order to obtain a rough estimation on T_e. Under such an assumption, the soft x-ray emission must be caused by electron bremsstrahlung in the ion field, and the total intensity of the radiation crossing an Al foil can be calculated as a function of the foil thickness, for the given value of T_e [19]. In figure 6 we present the experimental measurements of the x-ray intensity against the thickness of the Al foils in contrast with theoretical curves for several T_e values. Figure 6(a) corresponds to series of measurements performed on the emission from the plasma bulk, and figure 6(b) corresponds to the measurements performed on the bright points of the pictures only. Each experimental point corresponds to the average of around ten measurements, and the error bars represent the statistical dispersion. From figure 6(a) an electronic average temperature of the plasma bulk in the range 3–4 keV can be estimated. In the brilliant points the plasma seems highly non-Maxwellian. In fact, in figure 6(b) it can be seen that the experimental points go out to any curve. In the brilliant zones, ion and electron beams originate. It is not easy to deduce the electron-beam energy from measurements performed in the present work, but in previously published works [20, 21] ion beams were detected in the energy range of tens to several hundred kiloelectronvolts. The energy of the electron beam ejected in opposite direction to the ion beam must have similar value of energy, because both electron and ion beams would be accelerated by the same electric field.

3.2. Soft and hard x-ray emission against Y

The average time-integrated neutron yield Y, measured with the silver activation counters, was compared with time-resolved intensity measurements of soft x-ray (several keV) and hard x-ray (hundreds keV) radiated by the focus. The soft x-rays (intensity X_s) are normally associated with the bremsstrahlung emission of the plasma, and the hard x-ray emission (intensity X_h) is considered to be produced by the bombardment of the anode surface by the fast electron beams generated as a reaction of fast deuteron beams in the hot spots. These beams can be produced as a consequence of the spatial separation charges in the $m = 0$ instabilities observed in the focus. In other words, the X_h intensity is associated with beam-target effect. Figure 7 shows a three-dimensional graphic of the weighted average surface of Y against X_s and X_h that represents 300 discharges in the PACO device. Zone A is representative of high Y performance due to thermal fusion production. Zone B shows a good Y production by the beam-target effect, but less than zone A. Zone C represents the best Y production, where both effects are large. Zone D is an intermediate zone with both mechanisms working and zone E shows the drastic decrease of Y when X_s and X_h are low.

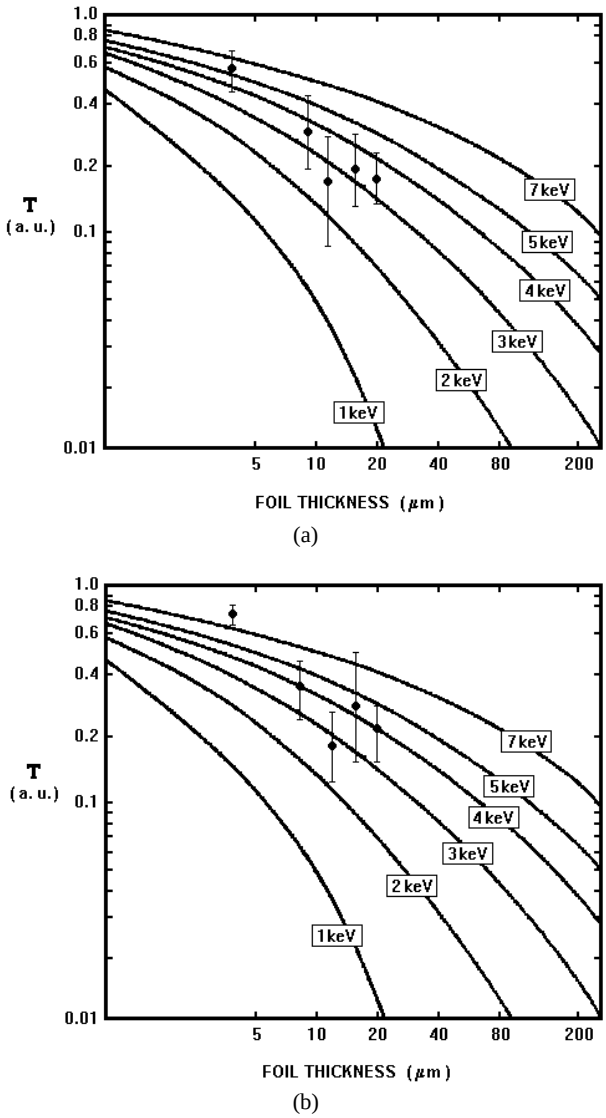

Figure 6. The x-ray transmittance against Al foil thickness: experimental points and theoretical curves (a) in the plasma bulk and (b) in the brilliant zones.

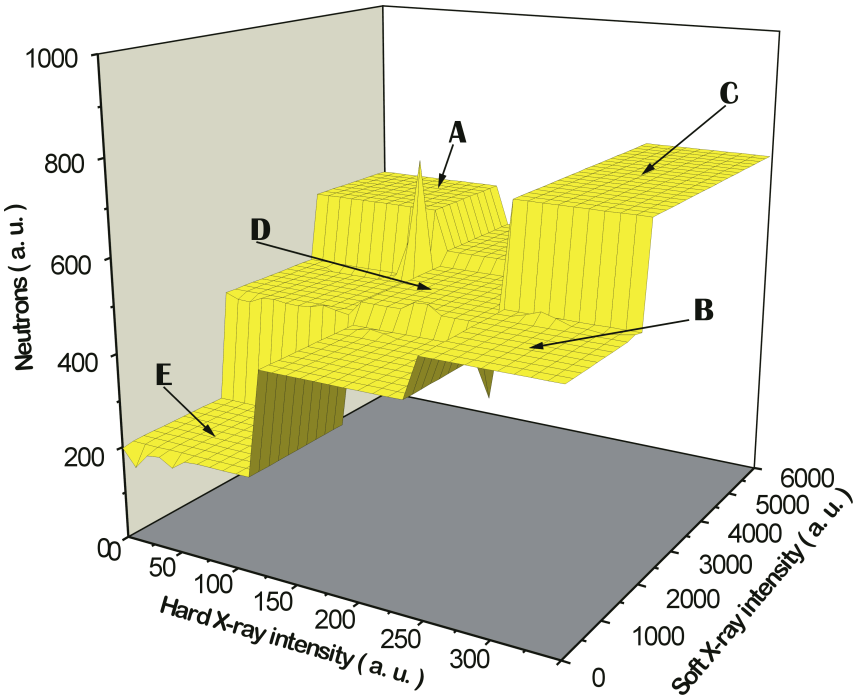

Figure 7. Three-dimensional graph of the weighted average surface of neutrons against soft and hard x-ray intensities representing three hundred discharges in the PACO device.

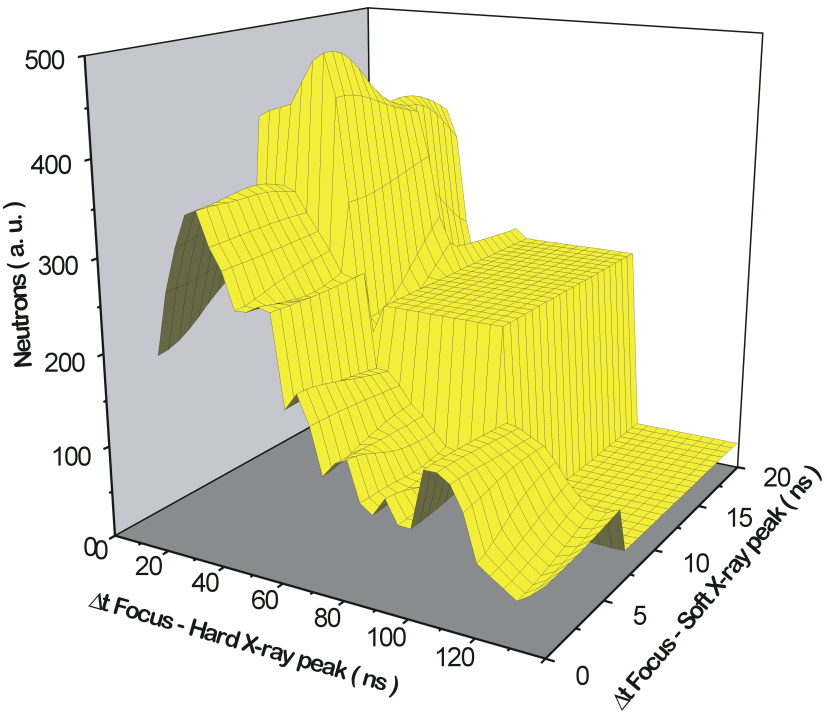

Figure 8. Three-dimensional graph of the weighted average surface of neutron yield against soft x-ray first peak time and hard x-ray peak time with respect to the dip time in the Rogowski signal.

3.3. The timing of soft x-ray intensity (X_s) and hard x-ray intensity (X_h) with the neutron yield Y

In figure 4 we can see two different oscilloscope registers: in figure 4(a) with only one peak in the soft x-ray signal and figure 4(b) with a second peak in this signal, separated from the first peak by several tens of nanoseconds. This second peak of soft x-rays appears with a frequency of ∼50% and does not correspond with a second peak in the hard x-ray signal (in all of the shots the hard x-ray signal presents only one peak). When a second peak of soft x-rays appears, in many of these cases (about 50%) it has a correspondence

with a second peak in dI/dt (see the signals in figure 4(b)). This means that the second soft x-ray emission may be mainly caused by a second compression of the column. Sometimes it produces a weak change in the current density, and dI/dt does not present, in these cases, a second dip.

In figure 8 we show the three-dimensional diagram of Y against the times of the first soft x-ray peak and hard x-ray peak (both taken respect to the dI/dt dip time t_0), represented by the weighted average surface defined from the three values measured shot-by-shot. As it can be seen, significant values of Y are obtained only when the first peak of soft x-ray appears in a narrow interval of 20 ns after t_0. With respect to the time of the hard x-ray peak, Y presents a maximum when this time is around 20 ns after t_0 and decreases strongly when the peak appear beyond 40–50 ns after t_0.

3.4. The time integrated neutron signal and soft x-ray signal

The maximum $Y(t)$ of the neutron pulse appears 50 ns after the first peak X_s (see figure 4(b)) in every shot. When a second x-ray burst appears, it does not correspond with a second neutron pulse. This means that the main neutron yield is produced in the first pinch compression. The half-width of the neutron pulse is 30–40 ns. The exponential decay of the neutron signal is not due to photomultiplier saturation. We interpret that this tail in the signal could be produced by the registration of neutrons scattered by the walls. However, this tail in the signal does not affect the main information obtained in the neutron pulse observation.

4. Conclusions and final remarks

The results of the investigations presented here—soft and hard x-ray emission and neutron yield—suggest that two types of mechanisms are present for neutron production: the beam-target effect (as evidenced by the measurement of hard x-rays from the impact of high-energy electron beams on the anode surface) and the thermal effect (as evidenced by the soft x-rays coming from electron bremsstrahlung in the thermal plasma). Both mechanisms can coexist, but seem to be independent of each other. This is deduced from the fact that sometimes there are meaningful Y values due to the beam-target effect (high x-ray emission) but not due thermal effect low soft x-ray emission). In other cases there are thermal evidences (high values of Y with high soft x-ray emission) and poor beam-target production (low hard x-ray emission). In another situation both of the mechanisms coincide (high intensity, both soft and hard, x-ray emission) with the higher neutron yield.

Some clear conclusions can be extracted from the results presented in figure 8. Significative values of Y are registered only when a soft x-ray pulse appears in the first 20 ns after the maximum compression (dip of dI/dt) and, especially, in the interval between 10 and 20 ns. This observation can give information, with temporal resolution, on the plasma temperature gradient produced by the current sheath kinetic energy randomization during the maximum pinch compression. On the other hand, the maximum values of Y are registered when X_h appears in temporal coincidence with the soft x-ray pulse. This fact suggests that the beam-target effect is more efficient when the beam is produced at the same time at which the plasma bulk reaches its maximum density (high target density in the plasma bulk).

The fact that the thermal fusion mechanism is, at least, so relevant to the beam-target effect, added to the fact that the thermal mechanism can quantitatively explain the empirical scaling law $Y \sim I^4$ [22], gives special interest to the perspective of plasma foci and z-pinches as alternative schemes in the nuclear fusion field.

Acknowledgments

We thank CONICET and the Buenos Aires Province Research Council (CICPBA) for their support for the stay of the Mexican researcher F Castillo-Mejía. Also, we thank the Instituto de Ciencias Nucleares (UNAM, México) for its support for our collaboration programme.

References

[1] Mather J W 1964 *Phys. Fluids* **7** (Supplement) S28–34
[2] Huddlestone R and Leonard S 1965 *Plasma Diagnostic Techniques* (New York: Academic) p 392
[3] Bernard A, Coudeville A, Jolas A, Launspach J and de Mascureau J 1975 *Phys. Fluids* **18** 180
[4] Bruzzone H, Gratton R, Kelly H, Milanese M and Pouzo J 1974 *Energy Storage, Compression and Switching Proc. Int. Conf. (Asti-Torino, 1974)* (New York: Plenum) p 255
[5] Milanese M and Pouzo J *Nucl. Fusion* **18** 533
[6] Lehner G and Pohl F 1967 *Z. Phys.* **207** 83
[7] Cipolla F 1968 LGI 68/23 *Internal Report* Laboratori Gas Ionizzati, Frascati, Italy
[8] Booth P 1956 *Proc. Phys. Soc.* **69** 265
[9] Mather J W 1971 *Methods of Experimental Physics* ed R H Lovberg and H R Grien (London: Academic) p 187
[10] Serban A and Lee S 1997 *Plasma Sources Sci. Technol.* **6** 78
[11] Jia Wang and Tsin-Chi Yang 1988 *J. Phys. D: Appl. Phys.* **21** 700
[12] Bourgade J L, Cavailler C, de Mascureau J and Miquel J L 1986 *Rev. Sci. Instrum.* **57** 2165
[13] Bostick W, Nardi V and Pryor W 1973 *J. Plasma Phys.* **8** 7
[14] Sadowski M, Herold H, Schmidt H and Shakhatre M 1984 *Phys. Lett.* A **105** 117
[15] Hirano K, Takahama Y, Han M and Yanagidaira T 1994 *J. Phys. Soc. Japan* **63** 3657
[16] Milanese M, Moroso R and Pouzo J 1993 *IEEE Trans. Plasma Sci.* **21** 373
[17] Rockett P, Bird C, Hailey C, Sullivan D, Brown D and Burkhalter P 1985 *Appl. Optics* **24** 2536
[18] Castillo-Mejia F, Milanese M, Moroso R and Pouzo J 1997 *J. Phys. D: Appl. Phys.* **30** 1499
[19] Herziger G 1984 *Springer Series in Optical Science* vol 43, ed G Schmahl and D Rudolph (Berlin: Springer) p 19
[20] Sadowski M, Skladnik-Sadowska E, Baranowski J, Milanese M, Moroso R and Pouzo J 1998 *J. Tech. Phys.* **39** 109
[21] Herold H, Jerzykiewicz A, Sadowski M and Schmidt H 1998 *Nucl. Fusion* **29** 1255
[22] Milanese M and Pouzo J 1988 *Small Plasma Physics Experiments* (London: World Scientific) p 66